

# Hills and holes in the microlensing light curve due to plasma environment around gravitational lens

Oleg Yu. Tsupko<sup>1</sup><sup>★</sup> and Gennady S. Bisnovatyi-Kogan<sup>1,2,3</sup><sup>†</sup>

<sup>1</sup>*Space Research Institute of Russian Academy of Sciences, Profsoyuznaya 84/32, Moscow 117997, Russia*

<sup>2</sup>*National Research Nuclear University MEPhI (Moscow Engineering Physics Institute), Kashirskoe Shosse 31, Moscow 115409, Russia*

<sup>3</sup>*Moscow Institute of Physics and Technology, 9 Institutskiy per., Dolgoprudny, Moscow Region, 141701, Russia*

Accepted XXX. Received YYY; in original form ZZZ

## ABSTRACT

In this paper, we investigate the influence of the plasma surrounding the gravitational lens on the effect of microlensing. In presence of plasma around the lens, the deflection angle is determined by both the gravitational field of the lens and the chromatic refraction in the inhomogeneous plasma. We calculate microlensing curves numerically for point-mass lens surrounded by power-law density distribution of plasma. A variety of possible curves is revealed, depending on the plasma density and frequency of observations. If the refractive deflection is large enough to compensate or overcome the gravitational deflection, microlensing images can completely disappear for observer. In this case, the remarkable effect occurs: formation of a 'hole' instead of a 'hill' in the center of microlensing light curve. In optical and near-infrared microlensing observations, the 'hill-hole' effect can be significant for lenses of small masses, which can be important for future observational projects.

**Key words:** gravitational lensing; micro – plasmas

## 1 INTRODUCTION

The theory of gravitational lensing deals usually with a propagation of light rays in vacuum. In vacuum, ray paths and deflection angles are independent on the photon frequency, and therefore all effects of gravitational lensing are achromatic. In particular, magnification curves for microlensing events are supposed to look the same at all wavelengths. Meanwhile, cosmic space is filled with plasma and plasma is also expected to be concentrated around compact objects. Under these conditions, a question arises: how does the plasma influence the phenomena of gravitational lensing?

In this article, we examine the effect of plasma on the microlensing phenomenon (for general discussion of microlensing see, e.g., [Schneider, Ehlers & Falco \(1992\)](#); [Schneider, Kochanek & Wambsganss \(2006\)](#); [Mao \(2012\)](#); [Dodelson \(2017\)](#); [Congdon & Keeton \(2018\)](#)). Presence of plasma leads to change of the deflection angle due to the effect of refraction. Moreover, since plasma is a dispersive medium, lensing becomes chromatic. Positions of images, magnification factors and, what is important for this arti-

cle, microlensing curves depend on the frequency at which observations are made.

Magnitude of plasma influence is determined by the ratio of the plasma frequency and the photon frequency. Lower photon frequency (longer wavelength) or higher plasma density leads to larger refractive deflection. Using the approximation that both angles are small, we calculate the total deflection of the ray as the sum of the gravitational deflection in vacuum and chromatic refraction in inhomogeneous plasma. Important feature of our analysis is that the plasma deflection is not assumed to be much smaller than the gravitational one.

When a light ray travels through the plasma atmosphere of a star or through the accretion disk around a black hole, the influence of the plasma on the light deflection can be significant due to the high concentration of the plasma. If the plasma deflection is large enough, it can fully compensate or overcome the gravitational deflection. In this paper, we show that the microlensing images can disappear (become invisible) because light rays from source will be diverged by the lens and will not reach the observer. This leads to the remarkable effect: formation of a 'hole' instead of a 'hill' in the center of microlensing light curve. We calculate the microlensing curves numerically for point-mass lens surrounded by power-law density distribution of plasma. A variety of possible curves is revealed, depending on the plasma den-

<sup>★</sup> E-mail: [tsupko@iki.rssi.ru](mailto:tsupko@iki.rssi.ru), [tsupkooleg@gmail.com](mailto:tsupkooleg@gmail.com) (OYuT)

<sup>†</sup> E-mail: [gkogan@iki.rssi.ru](mailto:gkogan@iki.rssi.ru) (GSBK)

sity and frequency of observations. Observational prospects depend on the lens mass, the plasma distribution and the frequency of observations involved. It is shown that in optical and near-infrared observations used for microlensing, the 'hill-hole' effect can be significant for lenses of small masses. This could be important for future observations in these bands.

The paper is organized as follows. In the next section we present the overview of previous results in research of plasma effects in gravitational lensing. In Section 3 we discuss the properties of overall deflection angle and approximations used. In Section 4 we introduce the lens equation in presence of both gravitational and refractive plasma deflections. In Section 5 we describe our method for numerical calculation of microlensing curve in presence of plasma. Sections 6 and 7 are devoted to results of numerical calculations for particular plasma density profiles. In Section 8 we discuss the observational prospects and derive the frequency window for possible observation where effect is significant. Section 9 is Conclusions.

## 2 GRAVITATIONAL LENSING IN PLASMA: STATE OF RESEARCH

For gravitational lensing, the main interest is the change in the deflection angle due to the presence of plasma. In the simplest case, when angles are small, we can separate gravitational and plasma deflections from each other, assuming that gravitational deflection is the same as in vacuum and plasma deflection is refractive deflection due to medium inhomogeneity. Under these conditions, to calculate the gravitational deflection angle, it is sufficient to use the linearized GR (which leads to the Einstein angle formula), and for refraction, we can assume that the refractive index of plasma is close to unity. In this approximation, the overall deflection angle was calculated in papers of Muhleman & Johnston (1966); Muhleman, Ekers & Fomalont (1970), in application to the deflection of radio signals in the plasma solar corona. The same approximation was subsequently used in book of Bliikh & Minakov (1989) who discussed different problems in context of gravitational lensing for the first time. In particular, the authors qualitatively discussed the number and the positions of the images.

In the approach described above, the deflections of light due to gravity and due to refraction in a non-homogeneous plasma were considered as small, and independent of each other effects. There are situations and problems when this approach is no longer enough. It happens, when the light travels close enough to the black hole, so that the light bending is not small. In addition, even a plasma with uniform density distribution can affect the magnitude of the gravitational deflection itself (Bisnovatyi-Kogan & Tsupko 2009).

The deflection angle is generally determined by a complex combination of effects of gravity, refraction and dispersion. More general consideration in general relativity of a light propagation in presence of medium was done by Synge (1960), and subsequently investigated by Bičák & Hadrava (1975) who first applied it for plasma, see also Kulsrud & Loeb (1992). Part of the monograph of Perlick (2000) is devoted to investigation of light ray propagation in presence of both gravity and plasma. In particular,

the exact expression for the deflection angle for the equatorial plane of the Kerr black hole was obtained in the form of integral.

Extensive study of gravitational lensing in presence of plasma has been started only about one decade ago. On basis of Synge's approach, the deflection angles in weak deflection case were derived, for light rays propagating in Schwarzschild metric in presence of non-homogeneous plasma (Bisnovatyi-Kogan & Tsupko 2009, 2010), see also Bisnovatyi-Kogan & Tsupko (2015). In particular, it has been shown that in a homogeneous plasma, where refractive deflection is absent, the gravitational deflection itself differs from vacuum case and depends on the photon frequency due to dispersive properties of plasma. For the case of homogeneous plasma, positions and magnifications of images were calculated analytically (Bisnovatyi-Kogan & Tsupko 2010). Er & Mao (2014) have continued studies of gravitational lensing in plasma in case of weak deflection taking into account vacuum gravitational deflection and refractive deflection in non-homogeneous plasma. They have performed a numerical modelling of a strong lens system and have shown that changes in the angular position of images due to refraction in plasma are possible to be detected in the low frequency radio observations.

In the case when a compact object, like a black hole or a neutron star, is surrounded by plasma, the rays of the light can experience a strong deflection. In the case of a gravitational lensing by a black hole, the rays can make one or more revolutions around it before reaching the observer. In presence of plasma, the properties of high-order images (also called relativistic (Virbhadra & Ellis 2000; Bozza et al 2001; Perlick 2004a)) formed by such rays have been analytically studied in the article of Tsupko & Bisnovatyi-Kogan (2013). A complex behavior of light rays near compact gravitating objects surrounded by inhomogeneous plasma was investigated in a series of works of Rogers (2015, 2016, 2017a,b). Curved ray paths were calculated numerically for various spherically symmetric power-law plasma distributions. Strong bending of light rays takes place also in the case of a shadow of black hole surrounded by plasma, see Perlick, Tsupko & Bisnovatyi-Kogan (2015), Perlick & Tsupko (2017), Huang, Dong & Liu (2018), Yan (2019).

For investigation of gravitational lensing in plasma in Kerr space-time we refer to Perlick (2000), Morozova, Ahmedov & Tursunov (2013), Perlick & Tsupko (2017), Liu, Ding & Jing (2017), Kimpson, Wu & Zane (2019a,b). For the wave effects in presence of Solar gravity and Solar corona, see Turyshev & Toth (2019a,b). For some recent studies see Schulze-Koops, Perlick & Schwarz (2017); Crisnejo & Gallo (2018); Crisnejo, Gallo & Rogers (2019); Er & Rogers (2018); Rogers & Er (2019); Er & Rogers (2019); Javed, Abbas & Övgün (2019); Sáreny and Balek (2019); Crisnejo, Gallo & Jusufi (2019). Recent review of plasma effects in gravitational lensing was made by Bisnovatyi-Kogan & Tsupko (2017).

## 3 OVERALL DEFLECTION ANGLE

Let us consider a photon flying past a spherical or point massive body of a mass  $M$  surrounded by a spherically sym-

metric plasma distribution with a number density  $N(r)$ . Assuming that the deflection angle of the photon is small, it can be written as the following function of the photon impact parameter  $b$ :

$$\hat{\alpha}(b) = \alpha_{grav}(b) + \alpha_{refr}(b). \quad (1)$$

Here the first term is the gravitational deflection in vacuum:

$$\alpha_{grav}(b) = \frac{4m}{b}, \quad (2)$$

where  $m = GM/c^2$  is the mass parameter. The second term in (1) is the non-relativistic refractive deflection.

Let us consider light rays in non-magnetized cold electron plasma with the refractive index

$$n^2 = 1 - \frac{\omega_p^2}{\omega^2}, \quad (3)$$

where

$$\omega_p^2 = K_e N, \quad K_e = \frac{4\pi e^2}{m_e}. \quad (4)$$

Here  $N$  is the number density of the electrons in the plasma,  $\omega_p$  is the electron plasma frequency,  $\omega$  is the photon frequency,  $e$  is the electron charge,  $m_e$  is the electron mass.

If the unperturbed path of the photon is parallel to the  $z$ -axis, deflection angle can be written as (Bisnovatyi-Kogan & Tsupko 2009, 2010, 2015):

$$\alpha_{refr}(b) = \frac{K_e}{\omega_0^2} \int_0^\infty \frac{\partial N}{\partial b} dz. \quad (5)$$

Here  $\omega_0$  is the photon frequency at infinity. Since we neglect the gravity in calculation of the refraction, there is no difference between frequency at infinity and at some other observer's position, so  $\omega_0$  equals to  $\omega$  in formula (3), see discussion below.

Properties of the overall deflection angle:

(i) In this paper, we consider gravitational deflection and refractive deflection as separate effects, and the overall deflection angle is calculated as a simple summation of two separate deflections. In this approximation, gravity does not influence the photon frequency in eq.(3). If we would like to go beyond such approximate approach (to consider a mutual influence of gravity and plasma, strong bending situations, black hole shadow etc), the influence of gravity on the photon frequency should be taken into account. In the rigorous approach (see Synge (1960); Bisnovatyi-Kogan & Tsupko (2010); Perlick, Tsupko & Bisnovatyi-Kogan (2015)), the photon frequency  $\omega$  in (3) is a frequency measured by a static observer at the position  $r$ , and it is a function of the space coordinates due to gravitational redshift. For example, for the Schwarzschild gravity,  $\omega(r)$  is connected with  $\omega_0$  as

$$\omega(r) = \frac{\omega_0}{\sqrt{1 - 2m/r}}. \quad (6)$$

In the exact calculations of deflection, the frequency  $\omega(r)$  should be used in (3) from the very beginning in all calculations. In our paper we use approximate approach, and in the refraction term we assume that  $\omega(r) \simeq \omega_0$ .

(ii) We also neglect here the plasma influence on the gravitational deflection itself, assuming that gravitational deflection is the same as in vacuum. Namely, we neglect corrections to the gravitational deflection associated with the

presence of plasma derived in Bisnovatyi-Kogan & Tsupko (2009, 2010). These corrections should not be confused with non-relativistic refractive terms. As in the previous comment, for calculation of these corrections, the refractive index (3) with (6) should be used.

(iii) In eq.(5), we have  $N = N(r)$  and  $r = \sqrt{b^2 + z^2}$ , so the expression under the integral sign is a function of  $b$  and  $z$ . To calculate the deflection angle, we perform partial differentiation with respect to  $b$  at constant  $z$ , and then, after integration along  $z$  at constant  $b$ , obtain deflection angle as the function of  $b$ .

(iv) Vacuum gravitational deflection is usually considered as positive, see (2). The refractive deflection (5) can be both positive or negative, depending on the density profile. Usually the density of plasma in different models decreases with radius ( $dN/dr < 0$ ), therefore the refractive deflection is usually opposite to the vacuum gravitational deflection: ( $\alpha_{refr}(b) < 0$ ).

(v) In the case of inhomogeneous plasma with a power-law number density

$$N(r) = N_0 \left( \frac{r_0}{r} \right)^k, \quad (7)$$

$$N_0 = \text{const}, \quad r_0 = \text{const}, \quad k = \text{const} > 1, \quad (8)$$

the refractive deflection is (Bliokh & Minakov 1989; Bisnovatyi-Kogan & Tsupko 2010, 2015)

$$\alpha_{refr}(b) = -\frac{K_e}{\omega_0^2} N_0 \left( \frac{r_0}{b} \right)^k \frac{\sqrt{\pi} \Gamma\left(\frac{k}{2} + \frac{1}{2}\right)}{\Gamma\left(\frac{k}{2}\right)}, \quad (9)$$

$$\Gamma(x) = \int_0^\infty t^{x-1} e^{-t} dt. \quad (10)$$

#### 4 LENS EQUATION IN PRESENCE OF GRAVITY AND PLASMA

For the axially symmetric mass distribution around a lens, the lens equation is one-dimensional. It connects the angular position  $\beta$  of a source and angular positions  $\theta$  of the lensed images through the deflection angle  $\hat{\alpha}$ , see Fig. 1a,b. For a general case of arbitrary positions of source, lens and observer and arbitrary magnitude of deflection angle, the lens equation can be found in Frittelli, Kling & Newman (2000), Perlick (2004b), Bozza (2008).

In most cases related with applications, the simplifications are used. First of all, all angles are supposed to be small:  $\beta, \theta, \hat{\alpha} \ll 1$ . The second, the distances between the source, lens, and observer are assumed to be much larger than the size of the lens (thin lens approximation).

Angles  $\beta$  and  $\theta$  are calculated from the line connecting the lens with an observer, see Fig. 1a,b. Usual convention is the following:  $\beta$  is supposed to be positive, and  $\theta$  can be both positive (image is on the same side from lens as a source) and negative (image is on the opposite side), see Fig. 1b. The case  $\beta = 0$  corresponds to perfect alignment of source, lens and observer; in this case the Einstein ring is formed. Photon impact parameter  $b$  and  $\theta$  are related by formula  $b = D_d |\theta|$ .

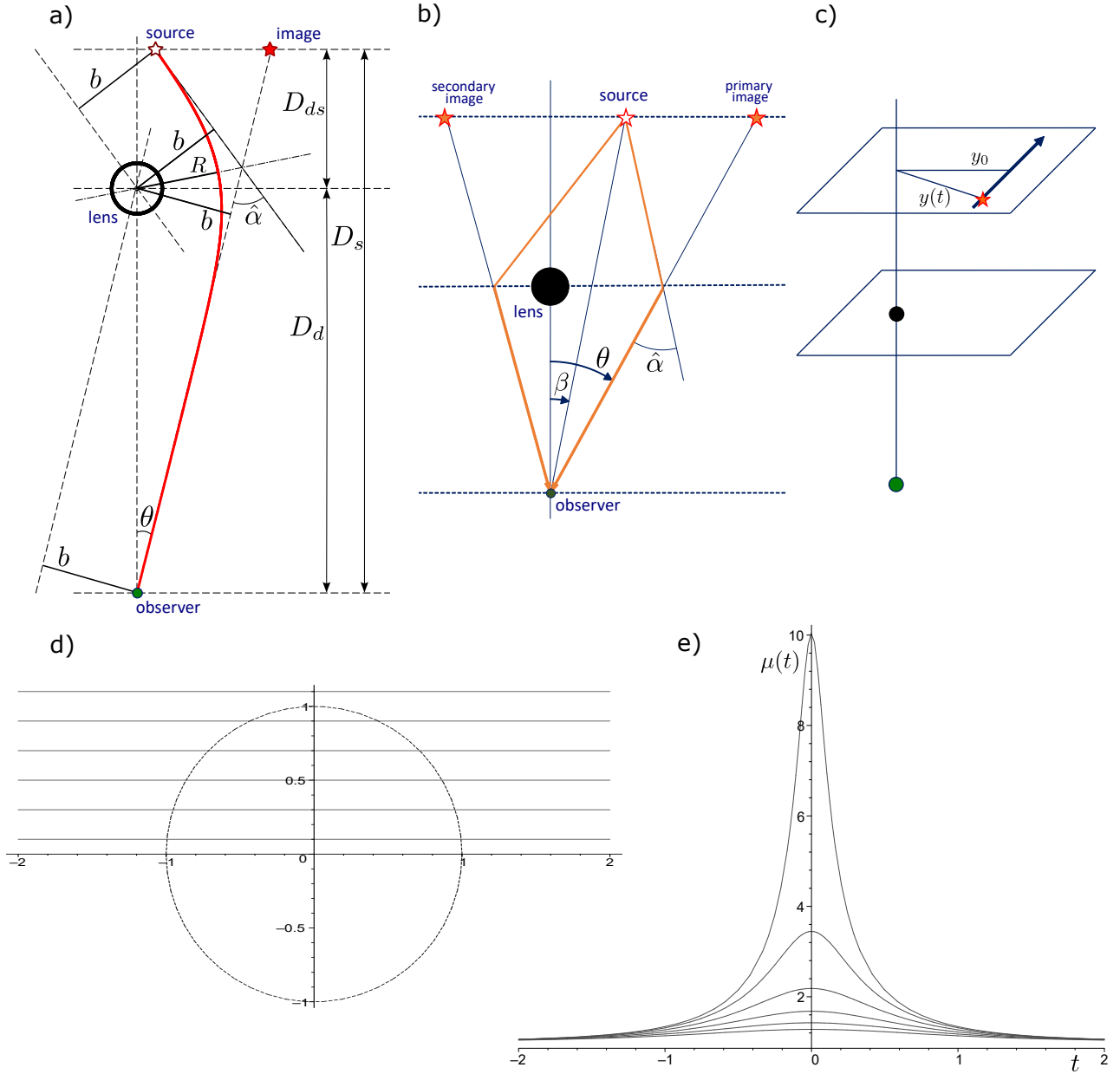


**Figure 1.** Effect of microlensing in vacuum. a) An example of the trajectory of a light ray calculated in vacuum. The impact parameter of the light ray  $b$  and the distance of the closest approach  $R$  are different values, but they are supposed to be equal in weak deflection approximation. b) Geometry of a point-mass lensing and notations in the lens equation. Two images are formed in the case of lensing in vacuum. c) Microlensing event: a source moves with the impact parameter  $y_0$  (in the normalized units) relative to the observer-lens axis. The value  $y_0$  should not be confused with the impact parameter  $b$  of the light ray. The instantaneous position of the source is given by  $y(t)$ , minimum of  $y(t)$  equals to  $y_0$ . d) Six trajectories of the source with different impact parameters, namely,  $y_0 = 0.1, 0.3, 0.5, 0.7, 0.9, 1.1$ . The dashed ring of unit radius corresponds to Einstein ring. e) Corresponding microlensing curves  $\mu(t)$  for impact parameters of the source shown in c). Higher curve corresponds to smaller impact parameter. See also Fig.2, page 458 of [Schneider, Kochanek & Wambsganss \(2006\)](#), and the interactive tool for plotting microlensing curves in the website 'microlensing-source.org'.

In approximations described above, the lens equation has a simple form:

$$\beta = \theta - \tilde{\alpha}(|\theta|) \frac{\theta}{|\theta|}, \quad (11)$$

where

$$\tilde{\alpha}(|\theta|) = \frac{D_{ds}}{D_s} \hat{\alpha}(D_d |\theta|). \quad (12)$$

Note that very often, the lens equation for axially symmetric case is written as  $\beta = \theta - \tilde{\alpha}(\theta)$ , see, e.g., eq.(35), p.31 in [Schneider, Kochanek & Wambsganss \(2006\)](#).

(2006). In such cases, it is assumed that the deflection angle has the property  $\tilde{\alpha}(-\theta) = -\tilde{\alpha}(\theta)$ , see eq.(36), p.32 in [Schneider, Kochanek & Wambsganss \(2006\)](#). In our case, the argument in the angle (1) has been supposed to be positive. Therefore, in order to correctly deal with the negative values of variable  $\theta$ , the lens equation is written as (11), see eq. (17) of [Suyu \(2012\)](#) and eq. (13), p.104 of [Schneider, Kochanek & Wambsganss \(2006\)](#), see also eq.(2.80) in [Congdon & Keeton \(2018\)](#).

In order to simplify eq.(11), let us introduce widely used normalized variables for the source and the image positions,

$$y = \frac{\beta}{\theta_E}, \quad x = \frac{\theta}{\theta_E}. \quad (13)$$

Here  $\theta_E$  is the vacuum Einstein angular radius

$$\theta_E = \sqrt{\frac{4mD_{ds}}{D_d D_s}}, \quad (14)$$

which corresponds to the angular size of the Einstein ring observed in the case of a perfect alignment.

We obtain in new variables:

$$y = x - \alpha(|x|) \frac{x}{|x|}, \quad (15)$$

with a normalized total deflection angle

$$\alpha(|x|) = \frac{1}{|x|} + \frac{1}{\theta_E} \frac{D_{ds}}{D_s} \alpha_{refr}(D_d \theta_E |x|). \quad (16)$$

Here the first term is simplified presentation for a gravitational deflection, the second term is connected with a refractive deflection. Combination  $D_d \theta_E |x|$  is an argument of  $\alpha_{refr}$ .

Below we consider only cases of the falling density profiles, for which  $\alpha_{refr} < 0$ . Therefore, for convenience, we introduce a positive function

$$B(|x|) \equiv -\frac{1}{\theta_E} \frac{D_{ds}}{D_s} \alpha_{refr}(D_d \theta_E |x|). \quad (17)$$

By physical meaning, the function  $B(x)$  is a refractive deflection angle taken with an opposite sign (normalized by distances ratio and by Einstein angular radius). This function is positive for profiles with a density decreasing with radial coordinate, and negative in the opposite case.

Using  $B(|x|)$ , the deflection becomes

$$\alpha(|x|) = \frac{1}{|x|} - B(|x|). \quad (18)$$

In the particular case of a power-law distribution (7) leading to the refractive deflection angle (9), the function  $B(|x|)$  can be represented as:

$$B(|x|) = \frac{B_0}{|x|^k}, \quad (19)$$

where we have introduced a constant

$$B_0 = \frac{1}{\theta_E} \frac{D_{ds}}{D_s} \frac{K_e}{\omega_0^2} N_0 \left( \frac{r_0}{D_d \theta_E} \right)^k \frac{\sqrt{\pi} \Gamma\left(\frac{k}{2} + \frac{1}{2}\right)}{\Gamma\left(\frac{k}{2}\right)}. \quad (20)$$

The constant  $B_0$  contains both values connected with a plasma and with a gravity, and characterizes the magnitude of the plasma influence in comparison with the gravitational

one. Using  $\omega_p^2(r) = K_e N(r)$ , it can be also rewritten as

$$B_0 = \frac{1}{\theta_E} \frac{D_{ds}}{D_s} \frac{\omega_p^2(D_d \theta_E)}{\omega_0^2} \frac{\sqrt{\pi} \Gamma\left(\frac{k}{2} + \frac{1}{2}\right)}{\Gamma\left(\frac{k}{2}\right)}. \quad (21)$$

Here the value  $D_d \theta_E$ , substituted as an argument of  $\omega_p$ , is the linear size of the vacuum Einstein ring.

Let us now discuss the properties of the lens equation (15) with (18) in different situations:

(i) In absence of plasma (ordinary gravitational lensing in vacuum), the deflection is

$$\alpha(|x|) = \frac{1}{|x|}, \quad (22)$$

and the well-known point-mass lens equation is recovered ([Schneider, Kochanek & Wambsganss 2006](#)):

$$y = x - \frac{1}{x}. \quad (23)$$

It has two solutions:

$$x_{\pm} = \frac{1}{2} \left( y \pm \sqrt{y^2 + 4} \right). \quad (24)$$

The solution  $x_+ > 0$  is usually called as a primary, it is located on the same side of the lens as the source. The secondary image,  $x_- < 0$ , is located on the opposite side of the lens, see Fig. 1a.

(ii) Our formalism can also allow to study lensing in the absence of the gravity, namely, so called plasma lensing. Plasma lensing is a diverging lensing by the compact distributions of plasma. In contrast to the converging achromatic behaviour of the vacuum gravitational lenses, the diverging frequency-dependent lensing occurs from the refraction of electromagnetic rays by the plasma along an observer's line of sight. Such plasma lensing has been recently studied numerically by methods of gravitational lens formalism in series of works of [Er & Rogers \(2018\)](#); [Rogers & Er \(2019\)](#); [Er & Rogers \(2019\)](#).

On the basis of the present approach, the normalized deflection angle for the plasma lensing is

$$\alpha(|x|) = -B(|x|), \quad (25)$$

and the lens equation has the following form:

$$y = x + B(|x|) \frac{x}{|x|}. \quad (26)$$

(iii) In the general case of simultaneous presence of gravity and plasma, the lens equation (15) with an overall deflection angle (18) can be solved only numerically. Each solution  $x_i$  of the lens equation gives us the image of the source.

Number of images depends on the plasma distribution and source position. This can be explained by plotting the right hand side of eq. (15), with account of (18), which we will denote as  $F(x)$ :

$$F(x) \equiv x - \alpha(|x|) \frac{x}{|x|}. \quad (27)$$

Every intersection of the horizontal line  $y$  (source position) with the curve  $F(x)$  determines a solution of the lens equation (15). Thus, the number of images is determined by the number of these intersections.



## 5 NUMERICAL CALCULATION OF THE MICROLENSING CURVE

In the axially symmetric case, the magnification factor (ratio of the flux from image, and from the unlensed source) can be written as (Schneider, Ehlers & Falco 1992; Schneider, Kochanek & Wambsganss 2006)

$$\mu_i = \frac{x}{y} \frac{dx}{dy}. \quad (28)$$

In the vacuum case of a point-mass lens, the magnification can be calculated fully analytically. The lens equation for the point-mass lens (23) can be solved analytically, which gives explicit functions of positions of two images,  $x_+(y)$  and  $x_-(y)$ , see (24). Substitution of  $x(y)$  into (28) allows to write down magnifications of every image as an explicit function of  $y$ .

The total magnification is a sum of two magnitudes of individual images, and is equal to (Schneider, Kochanek & Wambsganss 2006):

$$\mu = |\mu_1| + |\mu_2| = \frac{y^2 + 2}{y\sqrt{y^2 + 4}}. \quad (29)$$

The microlensing phenomenon is based on the change of the magnification with time due to the relative motion of the lens across the observer-source line-of-sight. The characteristic time scale of the magnification change is given by the Einstein time

$$t_E = \frac{D_d \theta_E}{v_\perp}, \quad (30)$$

where  $v_\perp$  is a transverse velocity of the lens relative to the source-observer line-of-sight (Schneider, Kochanek & Wambsganss 2006; Dodelson 2017; Congdon & Keeton 2018). Since the magnification (29) depends on the source position and the motion is relative, microlensing is described by the source motion relative to the lens (Schneider, Kochanek & Wambsganss 2006). Thus, during microlensing event, the source is moving and  $y$  is changing with time, see Fig. 1c. Usually the source trajectory is represented as (Schneider, Kochanek & Wambsganss 2006):

$$y(t) = \sqrt{y_0^2 + \left(\frac{t - t_0}{t_E}\right)^2}. \quad (31)$$

Here  $t_0$  is the time at which the source-lens separation  $y(t)$  is minimal,  $y(t_0) = y_0$ . The value  $y_0$  may be called as an impact parameter of the moving source (it should not be confused with the impact parameter  $b$  of the light ray). For simplicity, hereinafter we will take  $t_0 = 0$  and  $t_E = 1$ , which is equivalent to measuring of time in the units of  $t_E$ . Substituting  $y(t) = (y_0^2 + t^2)^{1/2}$  into (29), we obtain the microlensing curve  $\mu(t)$ . In Fig. 1e we plot the microlensing curves for different values of the source impact parameter  $y_0$ .

In the case of plasma presence, the lens equation is more complicated and cannot be solved analytically. It means that we cannot obtain an explicit function  $x(y)$  of each image. To calculate the magnification in this case, we rewrite eq.(28) as a function of  $x$  only. With a help of the lens equation (15), the magnification of each image takes form:

$$\mu_i^{-1} = \frac{y}{x} \frac{dy}{dx} \bigg|_{x=x_i} = \frac{F(x)}{x} \frac{dF(x)}{dx} \bigg|_{x=x_i}. \quad (32)$$

The advantage of this approach is that the analytical dependence  $F(x)$  is known (see eq.(27)), and the only value we need to calculate numerically is a solution of the lens equation,  $x_i$ . By formula (32), we obtain the magnification factor  $\mu_i$  of each image as a function of its angular position  $x_i$  found numerically. The total magnification is a sum of absolute values of all images magnifications:

$$\mu = \sum_i |\mu_i|. \quad (33)$$

For the reader convenience, we summarize the suggested method of the microlensing curve calculation in a step-by-step procedure:

1. Choose the distribution of the plasma number density  $N(r)$ , calculate the angle of the refractive deflection as a function of  $b$  by the formula (5), obtain the function  $B(|x|)$  by the formula (17), and substitute it into (18) and (15). For power-law density profiles (7), the function  $B(|x|)$  is given by (19) with the constant (20).

2. Fix some value of the impact parameter  $y_0$  of the source and present  $y$  as

$$y = \sqrt{y_0^2 + t^2}, \quad (34)$$

where  $t$  is the time in units of  $t_E$ .

3. Choose some interval of time. Then, for every  $t$  from this interval, solve the lens equation (15) numerically, which gives us a set of solutions  $x_i$  (the angular positions of the images).

4. Calculate  $\mu_i$  for every  $x_i$  by formula (32).

5. Calculate  $\mu$  by formula (33) and obtain the magnification curve  $\mu(t)$ .

## 6 MICROLENSING CURVES FOR POWER-LAW DENSITY PROFILE WITH $K = 3$

Let us start from the case of the power-law density profile with  $k = 3$ . This case is interesting because it allows analytical analysis of the lens equation (see the end of this section).

In this case, the plasma number density is:

$$N(r) = N_0 \left(\frac{r_0}{r}\right)^3. \quad (35)$$

Correspondingly, the function  $B(|x|)$  has a form:

$$B(|x|) = \frac{B_0}{|x|^3}, \quad (36)$$

and the lens equation can be presented as

$$y = x - \left(\frac{1}{|x|} - \frac{B_0}{|x|^3}\right) \frac{x}{|x|}, \quad (37)$$

or

$$y = x - \frac{1}{x} + \frac{B_0}{x^3}. \quad (38)$$

Results of the numerical calculation of microlensing events are shown in Fig. 2, where we plot the function  $F(x)$  (left column) and corresponding microlensing light curve (right column). The number of images is determined by the number of intersections of the horizontal line  $y$  with the curve  $F(x)$ . We choose a range of  $t$ -change, and during the microlensing event the value  $y$  changes from the maximum (the upper

horizontal line at left figures) value to the minimum value (the lower horizontal line), and then back. See caption of Fig. 2 for more details.

The vacuum case (Fig. 2a,b) corresponds to  $B_0 = 0$ , and for this case we always have two intersections of the horizontal line  $y$  with the function  $F(x)$ . Therefore we always have two images.

For small  $B_0$  (Fig. 2c,d) a new pair of images appears with small  $x$  (close to the lens). Therefore in this case we have four images. (We discuss mainly the range  $y \lesssim 1$ .) But the curve itself not much differs from the vacuum case.

For larger values of  $B_0$  (Fig. 2e,f) the change of the number of images ( $4 \rightarrow 2$ ) happens in the range  $y \lesssim 1$ , and the magnification curve noticeably changes.

For even larger values of  $B_0$  (Fig. 2g,h) there is a region when there is no intersections of  $y$  with  $F(x)$ , and there are no solutions of the lens equation. Therefore, for some time during microlensing event, the image is absent. This means that the diverging refractive deflection of the rays is becoming so strong that no ray from the source can reach the observer. In this case, in the center of the microlensing curve we have a 'hole' (instead of a 'hill'). The 'hole' of the same origin was found in the recent paper of [Er & Rogers \(2018\)](#) where they investigated the diverging refractive lensing by the compact distributions of plasma (in absence of the gravitational lens), see Figures 3,5,7 of that paper.

For  $k = 3$ , the formation of new images due to plasma presence and the complete disappearance of images in the case of a large refraction can be also investigated analytically, see the discussion in [Bliokh & Minakov \(1989\)](#).

For  $y = 0$  (perfect alignment of the source, lens and observer), Eq. (38) reduces to

$$0 = x - \frac{1}{x} + \frac{B_0}{x^3}, \quad (39)$$

and can be solved fully analytically. For  $B_0 = 0$  (vacuum) we have two solutions of different signs and of the same modulus,  $x = \pm 1$ , it is a vacuum Einstein ring. For  $0 < B_0 < 1/4$  we have four solutions:

$$x_{1,2} = \pm \frac{1}{2} \sqrt{2 + 2\sqrt{1 - 4B_0}} \quad (\text{first ring}), \quad (40)$$

$$x_{3,4} = \pm \frac{1}{2} \sqrt{2 - 2\sqrt{1 - 4B_0}} \quad (\text{second ring}). \quad (41)$$

For  $B_0 = 1/4$  four solutions merge into two solutions:

$$x_{1,2} = \pm \frac{\sqrt{2}}{2}, \quad (42)$$

so we have one ring. For  $B_0 > 1/4$  there are no solutions. It means that diverging refraction is so large that the images becomes invisible for observer. On Fig. 3 we present properties of these solutions.

## 7 MICROLENSING CURVES FOR POWER LAW DENSITY PROFILE WITH THE POWER 3/2

The power-law density distribution with  $k = 3/2$  is physically motivated, since it corresponds to spherically symmet-

ric accretion of free falling particles (dust), see Section VI in paper [Perlick, Tsupko & Bisnovatyi-Kogan \(2015\)](#).

The plasma number density is defined as

$$N(r) = N_0 \left( \frac{r_0}{r} \right)^{3/2}. \quad (43)$$

The function  $B(|x|)$  has a form:

$$B(|x|) = \frac{B_0}{|x|^{3/2}}, \quad (44)$$

and the lens equation can be presented as

$$y = x - \left( \frac{1}{|x|} - \frac{B_0}{|x|^{3/2}} \right) \frac{x}{|x|}. \quad (45)$$

Microlensing curves  $\mu(t)$  calculated with this density profile and different values of  $B_0$  are shown in Fig. 4. In general, all effects are the same as in Fig. 2.

## 8 OBSERVATIONAL PROSPECTS: FREQUENCY WINDOW

In this Section, we discuss the observational prospects and consider limitations on the frequency of observations associated with various physical effects, in particular with the Thomson scattering. As a result, we obtain a frequency window in which the discussed effects can be observed.

(i) Magnitude of effect:

to make the microlensing images invisible and to see a hole instead of a hill on the light curve, the refractive deflection should compensate or overcome the gravitational deflection. This happens at

$$|\alpha_{refr}(b)| > |\alpha_{grav}(b)|. \quad (46)$$

Using (2), (4) and (5) in (46), we write:

$$\frac{e^2}{m_e \omega_0^2} N_0 \frac{r_0^k}{b^k} > \frac{m}{b}. \quad (47)$$

( $m$  is the mass parameter,  $m = GM/c^2$ ). Let us rewrite it as ( $k > 1$ ):

$$\omega_0^2 < \frac{e^2}{m_e m} N_0 \frac{r_0^k}{b^{k-1}}. \quad (48)$$

To conclude, the 'hill-hole' effect is strong enough to be observable if  $\omega_0$  is smaller than the expression in right-hand side of (48).

(ii) Condition on the Thompson optical depth:

for the rays to reach the observer, plasma should be optically thin with respect to the Thomson scattering.

Let us consider the light ray whose unperturbed trajectory is a straight line parallel to the axis  $z$  with the impact parameter  $b$ . Thomson optical depth  $\tau$  for such trajectory and plasma distribution (7) is calculated as:

$$\tau = \int_{-\infty}^{\infty} \sigma N(r) dz = 2 \int_0^{\infty} \sigma N(r) dz = \quad (49)$$

$$= 2\sigma N_0 r_0^k \int_0^{\infty} \frac{dz}{(z^2 + b^2)^{k/2}} = \quad (50)$$

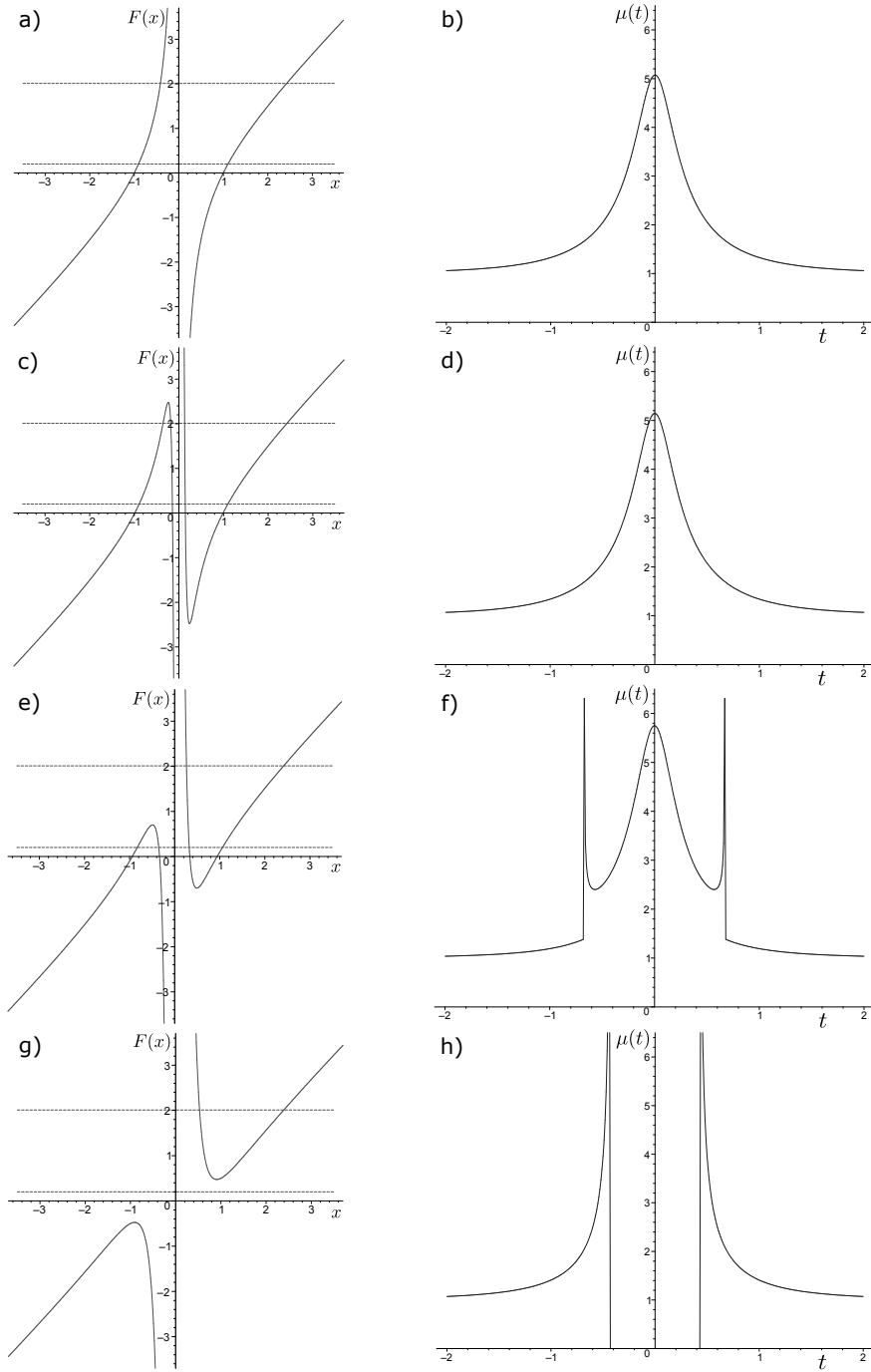


**Figure 2.** Microlensing curves in the case of a power-law distribution with  $k = 3$ , see eqs (35), (36), (38), plotted for different values of  $B_0$  which characterizes the plasma influence and is defined by (20). At the left column we plot the right hand side of lens equation (15), namely the function  $F(x)$  from (27), for some value of  $B_0$ . At the right column we plot the microlensing curve  $\mu(t)$  for this value of  $B_0$  using dependence  $y = (y_0^2 + t^2)^{1/2}$  with  $y_0 = 0.2$  and  $-2 \leq t \leq 2$ . The upper horizontal dashed line at the left figures is the value of  $y$  for  $t = \pm 2$ , on the lower horizontal line  $y = y_0$ , corresponding to  $t = 0$ . During the microlensing event, the value  $y$  changes from the upper to lower line, and then back. a,b)  $B_0 = 0$  (vacuum case). Here we always have two images, which leads to the usual gravitational microlensing curve. c,d)  $B_0 = 0.02$  (Influence of plasma is small.) For this value of  $B_0$ , there are always four images in the plotted range of  $t$ . In the plotted range of  $t$  the microlensing curve does not differ much from the vacuum case; the maximum of the curve becomes slightly higher. e,f)  $B_0 = 0.1$ . For this value, the change of number of images ( $4 \leftrightarrow 2$ ) happens during the change of  $y$ , which leads to noticeable change in the curve  $\mu(t)$ . g,h)  $B_0 = 0.5$ . For this value of  $B_0$ , the refraction is strong enough to make the images invisible for observer: for small enough values of  $y$  there are no solutions of the lens equation and, correspondingly, there are no images of the source. Therefore we have a 'hole' in the center of microlensing curve. High peaks in magnification curves (f,h) correspond to source crossing the caustics when the magnification becomes infinite and new pair of images appears or disappears (Schneider, Kochanek & Wambsganss 2006; Congdon & Keeton 2018; Alexandrov & Zhdanov 2011). If a simulation uses not a point source, but a source of a finite size, high peaks are smoothed.



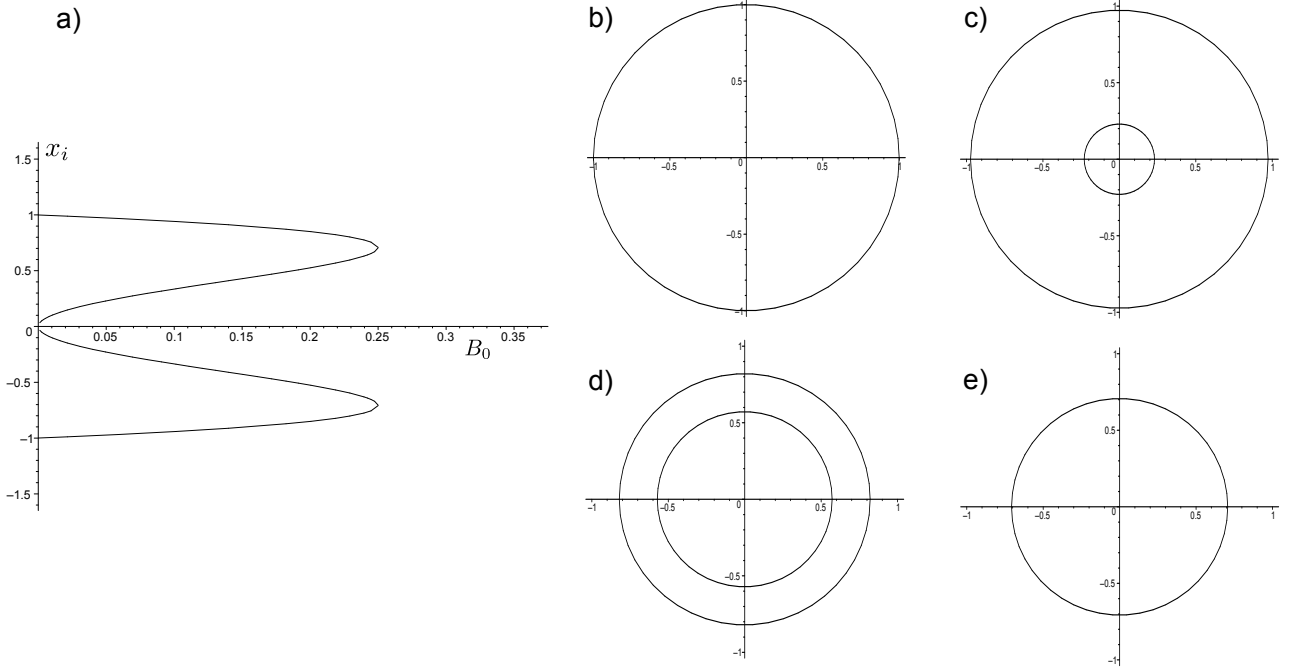


**Figure 3.** Ring-images in the case of a gravitational lensing in plasma, see also Fig. 2.19 in [Bliokh & Minakov \(1989\)](#). a) The dependence of four solutions  $x_i$  of equation (39) as functions of  $B_0$ . b)  $B_0 = 0$ . Einstein ring in vacuum. c)  $B_0 = 0.05$ . Two rings, the bigger one is smaller than vacuum Einstein ring. d)  $B_0 = 0.22$ . With increasing  $B_0$ , the large ring becomes smaller, and the small ring becomes larger. e)  $B_0 = 0.25$ . Two rings merge into one. For  $B_0 > 0.25$  there are no images.

$$= \sigma N_0 \frac{r_0^k}{b^{k-1}} \frac{\sqrt{\pi} \Gamma(k/2 - 1/2)}{\Gamma(k/2)}. \quad (51)$$

Here  $\sigma$  is Thomson cross section.

Thomson optical depth should be less than unity,

$$\tau < 1, \quad (52)$$

which leads to condition:

$$N_0 \frac{r_0^k}{b^{k-1}} < \frac{1}{\sigma}. \quad (53)$$

Substituting (53) into (48), we obtain finally:

$$\omega_0^2 < \frac{e^2}{m_e m \sigma}, \quad \text{or} \quad \omega_0^2 < \frac{e^2 c^2}{m_e G M \sigma}. \quad (54)$$

Numerical value is:

$$\omega_0 < 0.5 \cdot 10^{14} \left( \frac{M_\odot}{M} \right)^{1/2} \text{ s}^{-1}. \quad (55)$$

Using  $\lambda = 2\pi c/\omega_0$  (here we neglect the difference of light velocity in medium from vacuum), we obtain the following restriction for wavelength:

$$\lambda > 0.004 \left( \frac{M}{M_\odot} \right)^{1/2} \text{ cm}. \quad (56)$$

This means that observation of the hole (image disappearance) on the microlense curve is possible at conditions (55), (56), when Thompson scattering is still small.

(iii) For the wave to propagate in plasma, the photon frequency should be bigger than the plasma frequency,  $\omega_0 >$

$\omega_p$ . Numerically, we obtain the condition:

$$\omega_0 > 6 \cdot 10^4 \sqrt{N} \text{ s}^{-1}, \quad (57)$$

or

$$\lambda < 0.3 \cdot 10^7 \frac{1}{\sqrt{N}} \text{ cm}, \quad (58)$$

where  $N$  is measured in  $\text{cm}^{-3}$ .

(iv) Frequency window. Combining the conditions (55), (56), (57), (58), we obtain the frequency window of possible observation of the hole on the microlense curve

$$6 \cdot 10^4 \sqrt{N} \text{ s}^{-1} < \omega_0 < 0.5 \cdot 10^{14} \left( \frac{M_\odot}{M} \right)^{1/2} \text{ s}^{-1}, \quad (59)$$

or, equivalently,

$$0.004 \left( \frac{M}{M_\odot} \right)^{1/2} \text{ cm} < \lambda < 0.3 \cdot 10^7 \frac{1}{\sqrt{N}} \text{ cm}. \quad (60)$$

We are interested in consideration of masses of the order or smaller than the Solar mass and number densities bigger than  $1 \text{ cm}^{-3}$  (corresponds to interstellar medium). For such values, the frequency window of possible observation is rather big: there are several orders of magnitude between lower and upper limits in (60).

As discussed in previous studies ([Bisnovaty-Kogan & Tsupko 2009, 2010](#); [Er & Mao 2014](#); [Bisnovaty-Kogan & Tsupko 2017](#)), plasma effects in the strong lens systems are significant mainly for radio band. It is connected with relatively small plasma density in areas where the light propagates. Speaking about strong lens systems, plasma presence can provide only a small

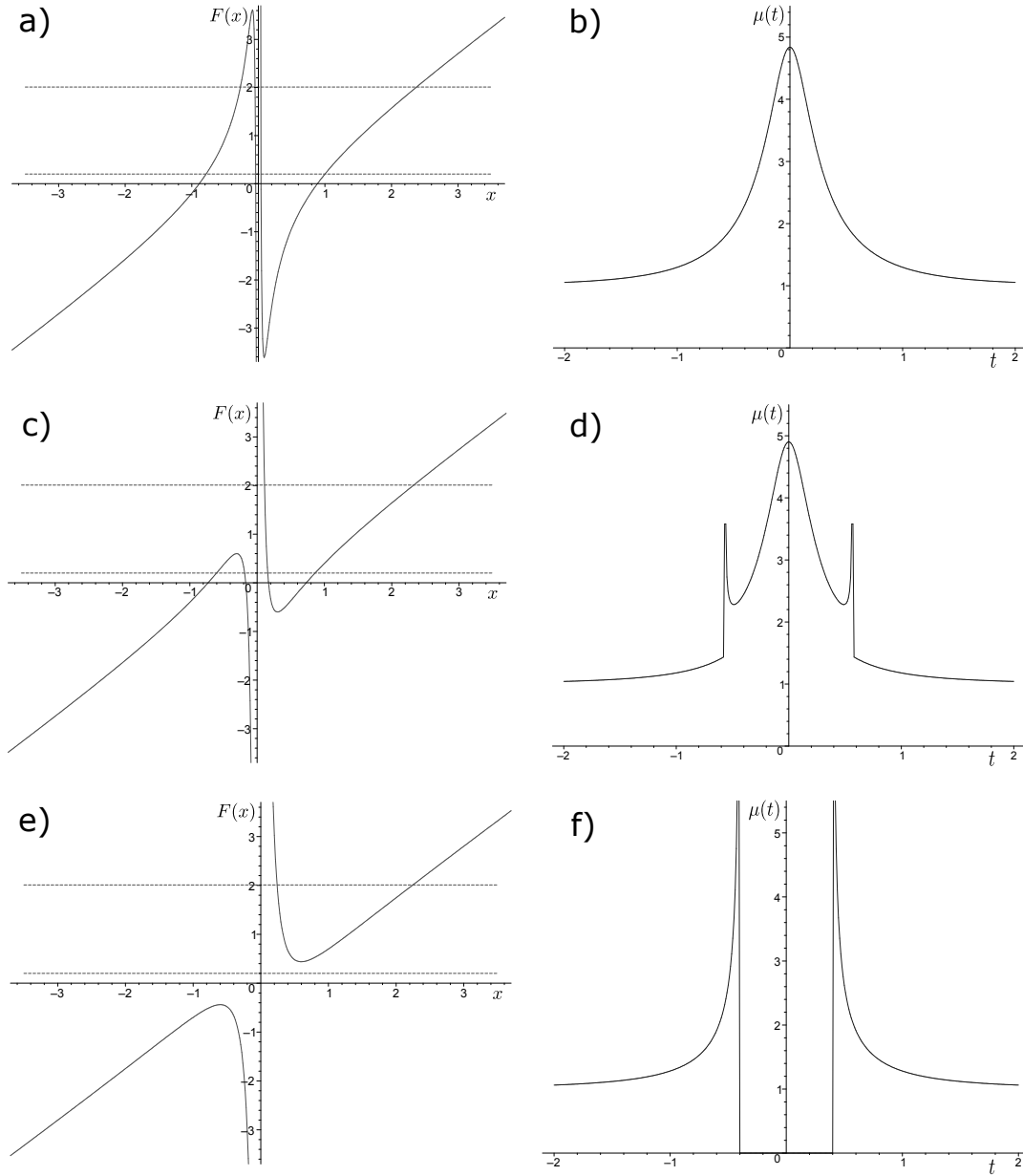


**Figure 4.** Microlensing curves in the case of a power-law distribution with  $k = 3/2$ , see eqs (43), (44), (45), plotted for different values of  $B_0$ ; for more details see the caption of the figure 2. a,b)  $B_0 = 0.2$ . For this value of  $B_0$ , there are always four images in the plotted range of  $t$ . In the plotted range of  $t$  the microlensing curve does not differ much from vacuum case; the maximum of curve becomes slightly smaller. c,d)  $B_0 = 0.4$ . For this value, the change of number of images ( $4 \leftrightarrow 2$ ) happens during the change of  $y$ , which leads to noticeable change in the curve. e,f)  $B_0 = 0.7$ . For this value of  $B_0$ , the refraction is strong enough to make the images invisible for observer. Therefore we have a hole in the center of microlensing curve.

change in positions and magnifications of images in comparison with the vacuum case. Here, in case of microlensing, the situation is more favorable. When a light ray travels through the plasma atmosphere of a star or through the accretion disk around a black hole, the refraction can be significant. For power-law dependence, the gravitational deflection can be overcome by the refraction if we consider small enough impact parameters. The light trajectory is determined by the significant influence of both gravity and plasma refraction. Therefore the refraction can significantly

influence the physical situation: the images can completely disappear (become invisible).

In case of microlensing, we are interested not in radio but mainly in optic (and also infrared) band. It can be seen from the condition (56) that in order to get into the infrared or optical band, it is necessary to consider lenses of sufficiently small masses.

Considering compact object with mass of dozen of Jupiter's masses (about 1/100 of Solar mass), we conclude that 'hill-hole' effect can influence the microlensing events observed in the infrared range:  $\lambda > 4 \mu\text{m}$ .

The planned project WFIRST (Spergel et al 2015) will extend the current sensitivity of the microlensing method down to masses of about a tenth of the Earth's mass. Observations will be performed in optical and near-infrared bands. Considering lens with mass of  $10^{-6}M_{\odot}$ , we obtain:  $\lambda > 40$  nm, (in particular, this covers the optical band). It means that plasma effect may significantly influences microlensing curves for lens of such small masses.

## 9 CONCLUSIONS

(i) The influence of the plasma surrounding the lens on the effect of microlensing is investigated. In the presence of plasma around the lens, the deflection angle is determined by both the gravitational field of the lens and the chromatic refraction in the inhomogeneous plasma.

(ii) Lens equation for lensing in presence of gravity and non-homogeneous plasma is presented. In our approximations, both gravitational and refractive deflections are small, but the plasma deflection is not assumed to be much smaller than the gravitational one.

(iii) Microlensing curves are calculated numerically for point-mass lens and two power-law density distributions of plasma, namely for  $k = 3$  and  $k = 3/2$ . A variety of possible curves is found, depending on the plasma density and frequency of observations.

(iv) For small magnitudes of plasma influence, the microlensing curve does not differ much from vacuum case. The maximum of curve in presence of plasma may be both higher and lower in comparison with vacuum case, depending on the plasma density distribution.

(v) If the refractive deflection is large enough to compensate or overcome the gravitational deflection, microlensing images can completely disappear for observer due to divergence of rays. In this case, the 'hole' instead of the 'hill' is formed in the center of microlensing light curve, which can be important for future observations.

(vi) In presence of plasma, the shape of microlensing curve depends on the frequency of observations. In optical and near-infrared observations which are used for microlensing, 'hill-hole' effect can be significant for lenses of small masses. This can be important for future projects like WFIRST.

## ACKNOWLEDGMENTS

We are thankful to Dr Alexander Polnarev for useful and pleasant discussions.

The reported study was funded by Russian Foundation for Basic Research (RFBR), project number 17-02-00760.

## REFERENCES

Alexandrov A. N., Zhdanov V. I., 2011, MNRAS, 417, 541  
 Bičák J., Hadrava P., 1975, A&A, 44, 389.  
 Bisnovatyi-Kogan G. S., Tsupko O. Yu., 2009, Gravitation and Cosmology, 15, 20  
 Bisnovatyi-Kogan G.S., Tsupko O.Yu., 2010, MNRAS, 404, 1790.  
 Bisnovatyi-Kogan G.S., Tsupko O.Yu., 2015, Plasma Phys. Rep., 41, 562.

Bisnovatyi-Kogan G.S., Tsupko O.Yu., 2017, Universe, 3, 57  
 Bliokh P. V., Minakov A. A., 1989, Gravitational Lenses. Naukova Dumka, Kiev (in Russian)  
 Bozza V., Capozziello S., Iovane G., Scarpetta G., 2001, General Relativity and Gravitation, 33, 1535  
 Bozza V., 2008, Phys. Rev. D, 78, 103005  
 Congdon A.B., Keeton C., 2018, Principles of Gravitational Lensing: Light Deflection as a Probe of Astrophysics and Cosmology, Springer International Publishing  
 Crisnejo G., Gallo E., 2018, Phys. Rev. D, 97, 124016  
 Crisnejo G., Gallo E., Jusufi K., 2019, eprint arXiv: 1910.02030  
 Crisnejo G., Gallo E., Rogers A., 2019, Phys. Rev. D, 99, 124001  
 Dodelson S., 2017, Gravitational Lensing, Cambridge University Press, Cambridge, UK  
 Er X., Mao S., 2014, MNRAS, 437, 2180.  
 Er X., Rogers A., 2018, MNRAS, 475, 867  
 Er X., Rogers A., 2019, MNRAS, 488, 5651  
 Frittelli S., Kling T. P., and Newman E. T., 2000, Phys. Rev. D, 61, 064021  
 Huang Y., Dong Y.-P., Liu D.-J., 2018, International Journal of Modern Physics D, 27, 1850114  
 Javed W., Abbas J., and Övgün A., 2019, Phys. Rev. D, 100, 044052  
 Kimpson T., Wu K., Zane S., 2019a, MNRAS, 484, 2411.  
 Kimpson T., Wu K., Zane S., 2019b, MNRAS, 486, 360  
 Kulsrud R. and Loeb A., 1992, Phys. Rev. D, 45, 525.  
 Liu C., Ding C., Jing J., 2017, Chinese Physics Letters, 34, 090401.  
 Mao S., 2012, Res. Astron. Astrophys., 12, 947.  
 Morozova V.S., Ahmedov B.J., Tursunov A.A., 2013, Ap&SS, 346, 513.  
 Muhleman D.O., Johnston I.D., 1966, Phys. Rev. Lett., 17, 455.  
 Muhleman D.O., Ekers R.D., Fomalont E.B., 1970, Phys. Rev. Lett., 24, 1377  
 Perlick V., 2000, Ray Optics, Fermat's Principle and Applications to General Relativity. Springer, Heidelberg, Germany  
 Perlick V., 2004a, Living Rev. Relativ., 7, 9.  
 Perlick V., 2004b, Phys. Rev. D, 69, 064017  
 Perlick V., Tsupko O.Yu., Bisnovatyi-Kogan G.S., 2015, Phys. Rev. D, 92, 104031.  
 Perlick V., Tsupko O.Yu., 2017, Phys. Rev. D, 95, 104003.  
 Rogers A., 2015, MNRAS, 451, 17.  
 Rogers A., 2016, arXiv:1611.00076.  
 Rogers A., 2017a, MNRAS, 465, 2151.  
 Rogers A., 2017b, Universe, 3, 3.  
 Rogers A., Er X., 2019, MNRAS, 485, 5800  
 Sárený M. and Balek V., 2019, eprint arXiv: 1907.08525  
 Schneider P., Ehlers J., Falco E., 1992, Gravitational lensing. Springer-Verlag, Berlin  
 Schneider P., Kochanek C.S., Wambsganss J., 2006, Gravitational Lensing: Strong, Weak and Micro, Swiss Society for Astrophysics and Astronomy Series: Saas-Fee Advanced Courses, Number 33, Springer, Berlin  
 Schulze-Koops K., Perlick V. and Schwarz D.J., 2017, Classical and Quantum Gravity, 34, 215006.  
 Spergel D., Gehrels N., Baltay C., et al, 2015, eprint arXiv: 1503.03757  
 Suyu S. H., 2012, MNRAS, 426, 868  
 Synge J. L., 1960, Relativity: the General Theory. North-Holland Publishing Company, Amsterdam  
 Tsupko O. Yu., Bisnovatyi-Kogan G. S., 2013, Phys. Rev. D, 87, 124009.  
 Turyshev S. G., Toth V. T., 2019a, Journal of Optics, 21, 045601  
 Turyshev S. G., Toth V. T., 2019b, Phys. Rev. D, 99, 024044  
 Virbhadra K. S., Ellis G. F. R., 2000, Phys. Rev. D, 62, 084003  
 Yan H., 2019, Influence of a plasma on the observational signature of a high-spin Kerr black hole, Phys. Rev. D, 99, 084050

This paper has been typeset from a  $\text{\TeX/L\AA\TeX}$  file prepared by the author.